Forward bias degradation and thermal simulations of vertical geometry β-Ga$_2$O$_3$ Schottky rectifiers

Minghan Xian, Randy Elhassani, Chaker Fares, Fan Ren, Marko Tadjer, and S. J. Pearton

Forward bias degradation and thermal simulations of vertical geometry β-Ga$_2$O$_3$ Schottky rectifiers

Minghan Xian,[1] Randy Elhassani,[1] Chaker Fares,[1] Fan Ren,[1] Marko Tadjer,[2] and S. J. Pearton[3,a]

[1]Department of Chemical Engineering, University of Florida, Gainesville, Florida 32611
[2]US Naval Research Laboratories, Washington, DC 20375
[3]Department of Material Science and Engineering, University of Florida, Gainesville, Florida 32611

Vertical geometry β-Ga$_2$O$_3$ Schottky rectifiers of various sizes were deliberately stressed at a high forward current density level until a sudden decrease of reverse bias breakdown voltage was observed. The diodes were fabricated on an Sn-doped (n = 3.6 × 10^{18} cm^{-3}) (001) β-Ga$_2$O$_3$ single crystal substrate with a 10 μm epilayer grown by halide vapor phase epitaxy with a carrier concentration of 3.5 × 10^{16} cm^{-3}. The forward bias stressing caused reverse breakdown degradation and thermally induced failure on both the Ni/Au Schottky contact and the epitaxial layer due to the low thermal conductivity of Ga$_2$O$_3$. The resulting temperature distributions at forward bias under different current conditions were simulated using 3D finite element analysis. The temperature profile at the surface during the rectifier turn-on period shows a strong dependence with crystalline orientation, evidenced by infrared camera measurements. The maximum junction temperature rise occurs at the center of the metal contact and is in the range of 270–350 °C. *Published by the AVS.*
https://doi.org/10.1116/1.5127511

I. INTRODUCTION

β-phase Ga$_2$O$_3$ is attracting interest for high-power electronics applications. The ultrawide bandgap for β-Ga$_2$O$_3$ (4.6–4.9 eV) leads to a higher breakdown field strength (7–8 MV/cm) and provides a higher Baliga figure-of-merit compared to other commercially available wide bandgap materials, for example, 4H SiC and GaN.[1–8] The low on-state loss and higher reverse voltage blocking capacity of β-Ga$_2$O$_3$ rectifiers may enable this material to become a major competitor in the sector of the power electronic market, such as avionics and space applications, as well as inverter modules in electrical motored vehicle and power management systems.[1–5]

Although it is a promising candidate for the high-power electronics market, the low thermal conductivity (27 W/m K on the [010] direction and 11 W/m K on the [110] direction) remains a limitation compared to GaN (210 W/m k) and SiC (270 W/m k).[2,5–7] Schottky diodes fabricated on β-Ga$_2$O$_3$ have already demonstrated a reverse breakdown of 2500 V, >30 A of absolute forward current, and >1 A in diode switching performance.[9–29] To achieve a high reverse blocking capability, a low doped n-type epitaxial layer is required, which leads to lower electrical conductance and in turn exacerbates heat generation in the epitaxial layer.[30] Under deliberately induced failure at high current forward bias conditions, cracks may appear on the Schottky contact, and delamination along the [010] crystal orientation has been observed.[11] The failure mechanism has been mainly ascribed to the plastic deformation of the lattice structure owing to device self-heating. Previous thermal simulations have shown that the main mechanism of heat generation in a vertical β-Ga$_2$O$_3$ Schottky device is Joule heating, and the highest temperature was observed near the metal-epi interface.[17–19] Therefore, optimized thermal management has become a key consideration for advancement in device performance and mitigation of potential device failure under high-power operation conditions. Clearly, effective thermal management approaches are needed. Noteworthy is a recent demonstration of top-gate nanomembrane Ga$_2$O$_3$ field effect transistors on a diamond substrate.[25] These devices exhibited a high maximum drain current of 980 mA/mm and 60% less temperature increase from reduced self-heating, compared to similar devices on the sapphire substrate at the same identical power density.

For advancement in β-Ga$_2$O$_3$ electronic devices, fabrication of the reliable Schottky contact with the ability to operate at high current density and high temperature is needed. It is also crucial to develop an understanding of the failure mechanism as a result of device self-heating. In this work, we report experimental measurements and steady state thermal simulations of vertical β-Ga$_2$O$_3$ rectifiers under high forward current density conditions which are found to induce reverse breakdown failure and crystalline structural deformation.

II. EXPERIMENT

The diodes were fabricated on a 10 μm Si-doped (3.5 × 10^{16} cm^{-3} confirmed with capacitance-voltage measurements) epitaxial layer grown by halide vapor epitaxy on (001) orientated 650 μm β-phase Sn-doped (n = 3.6 × 10^{18} cm^{-3}) Ga$_2$O$_3$ with an edge-defined film-fed growth method (Novel Crystal Technology). A backside Ohmic contact (20 nm/80 nm Ti/Au) was formed using an electron beam (e-beam) evaporation followed by 30 s rapid thermal annealing at 550 °C in nitrogen ambient using an SSI SOLARIS 150 rapid thermal annealer.

40 nm Al$_2$O$_3$ and 360 nm SiN$_x$ dielectric were deposited on the sample surface using Cambridge-Nano-Fiji atomic
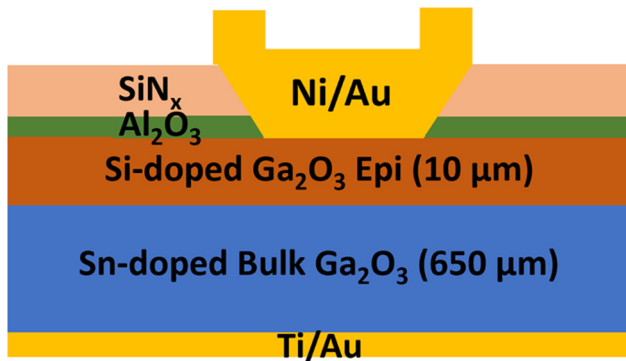
a)Electronic mail: spear@mse.ufl.edu

FIG. 1. Schematic of the rectifier structure used in these experiments.

TABLE I. Thermal conductivity and heat transfer coefficient for materials used in simulation.

Material	Thermal conductivity (W/m K)
Metal contact (gold)	315
Heat sink (copper)	380
β-Ga$_2$O$_3$—[001] direction	$18\,765 \times T$ (K)$^{-1.26}$
β-Ga$_2$O$_3$—[010] direction	$659\,992 \times T$ (K)$^{-1.77}$
β-Ga$_2$O$_3$—[100] direction	$11\,078 \times T$ (K)$^{-1.21}$
Convective heat transfer coefficient: 10 W/m^2 K	

layer deposition and Plasma-Therm plasma enhanced chemical vapor deposition tools, respectively. Dielectric windows with different sizes (0.8–0.2 mm squares, 0.2–0.04 mm diameter circles) were opened using 1:10 diluted buffered oxide etchant. The sample surface was then treated in O$_3$ for 20 min to remove hydrocarbon and other contamination species. 400 μm Ni/Au (80 nm/320 nm) Schottky metal was subsequently deposited using e-beam evaporation with standard acetone lift-off. A schematic of the device structure is shown in Fig. 1. The purpose of having circular and square contacts was to examine whether the geometry affects the ability to withstand electrical stressing, due to the significant anisotropy in thermal conductivity in Ga$_2$O$_3$. 800–200 μm length squares and 200–40 μm diameter circles were fabricated on the same wafer, since designing diodes with rounded geometry will effectively mitigate the electric field at the perimeter of the device, hence increasing the diode breakdown capability. On the other hand, designing diodes at square geometry will provide a larger contact surface area compared to circles of the same diameter, thus increasing the absolute current density for the device as shown by >1 A of absolute forward current for 800 μm^2 in this work.

For diode DC characteristics, a Tektronix 370-A curve tracer was used for forward and reverse I-V measurements. For diode stress measurements, an Agilent Technologies 8114A pulse generator was used to apply continuous voltage bias at 95% duty cycle for 1 min at various voltage levels. Thermal images of the sample were taken using an Optris PI640 infrared camera.

III. SIMULATIONS

For thermal simulation, a 3D finite element analysis was employed to calculate the temperature distribution with a steady state energy balance equation using rectangular coordinators (x-, y-, and z-axes),[31]

$$k_x \frac{\partial^2 T}{\partial x^2} + k_z \frac{\partial^2 T}{\partial y^2} + k_z \frac{\partial^2 T}{\partial z^2} + Q = 0, \qquad (1)$$

where T is the temperature; t is the time; Q is the source of power; k_x, k_y, and k_z are the substrate thermal conductivity for the x, y, and z directions, respectively. The heat

generation term, Q, was calculated using device forward current and empirical device on-resistance. For the boundary conditions, the bottom of the diode was connected to a copper heat sink was set to be ambient temperature. The heat dissipation for the top surface and the periphery of the device was governed by natural convection by air,

$$q = hA(T_s - T_{amb}), \qquad (2)$$

where q is the overall heat convection rate, h is the convective heat transfer coefficient of air, A is the surface area of convection, T_s is the surface temperature, and T_{amb} is the ambient temperature. The respective values and correlations for thermal conductivity and heat transfer coefficient are tabulated in Table I.[5–7]

The steady state temperature contours of diodes with various geometries ranging from $800 \times 800\,\mu$m^2 to 200, 100, and 40 μm diameter circles were simulated with different operating powers. The highest junction temperature at the center of the metal contact was used to compare the temperature rise at various current density levels and device sizes.

IV. RESULTS AND DISCUSSION

The forward current-voltage (I-V) and current density-voltage (J-V) characteristics for Schottky contacts of different sizes are shown in Fig. 2. Various contact sizes were used, ranging from 800 μm square to 40 μm circle in order to examine the correlation between contact geometry and operating conditions at which the rectifying performance fails due to high forward voltage bias. The Schottky barrier height of 1.05 eV with an ideality factor of 1.05 was extracted from the linear portion of the curve, which is in agreement with the previously reported values for Ni/Au contacts.[27,32,33] Rectifiers of different sizes were stressed via using a pulse generator pulsed for 1 min at 95% duty cycle at a constant voltage. The forward voltage was increased gradually by 1 V until a sudden irreversible increase of the reverse bias leakage current and an irreversible decrease of breakdown occurred at a given reverse bias voltage. Figure 1(b) shows the current density at degradation, which is a strong function of contact size. For the largest diodes (0.8 mm square), the diodes degrade at around 185 A/cm^2 forward current density, while the smallest diodes (40 μm diameter circle) is able to sustain higher current density up to 2100 A/cm^2 at about 20 V. This is
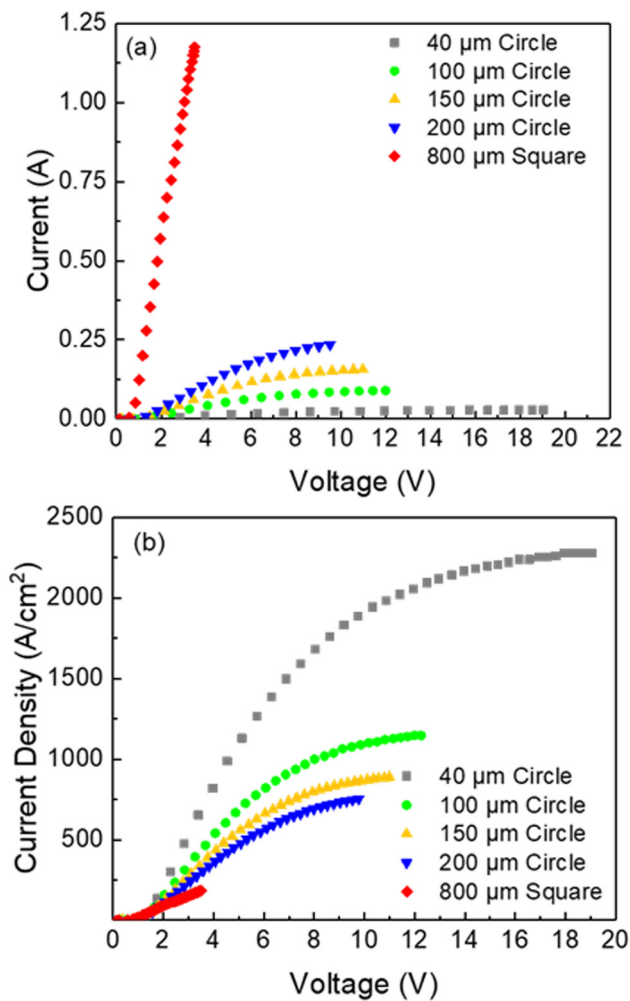
FIG. 2. Diode forward I-V (a) and J-V (b) characteristics for various size diodes until point of failure.

a significant result showing that the current state-of-the-art fabrication technique for β-Ga$_2$O$_3$ diodes can not only produce forward current at >1 A but also sustain high current density above 2 kA/cm^2 prior to failure. The size dependent diode

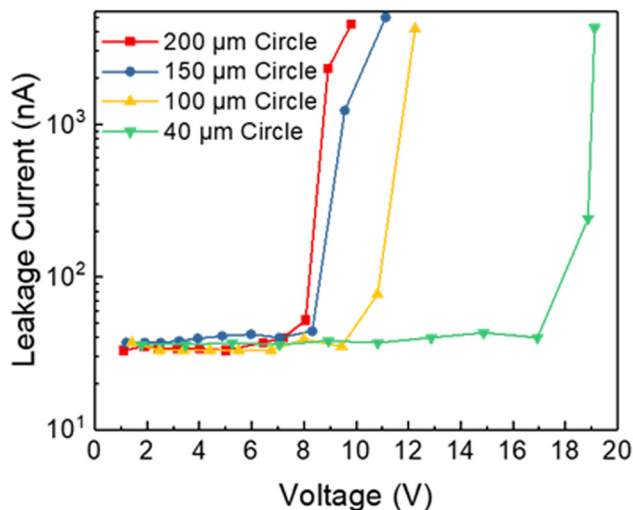failure current density results from the current crowding effect due to the spreading resistance on the metal contact, and heat generation as well as dissipation through the rectifiers.[30] Sharma *et al.*[30] also discussed the effect of epi and substrate thickness on the thermal profiles within vertical rectifiers. Yang *et al.*[26] have reported interconnected multiple diodes with a total area of 0.09 cm^2, achieving 33 A of absolute forward current at a sweep condition with a current density of 376 A/cm^2, where the current density is still an order of magnitude below that reported in this work.[26]

Figure 3 shows the diode reverse leakage current of different rectifier sizes at 100 V reverse bias as a function of forward bias step-stressed voltage for 1 min at 95% duty cycle until a sudden catastrophic increase of diode leakage current occurred at specific voltages. The strong size dependence for diode degradation indicates that the dissipation of heating for vertical geometry device remains a major issue for high power application. Figures 4(a) and 4(b) show the device reverse I-V characteristics for rectifiers both as deposited and after failure via step-stress, respectively. Ni/Au diodes of various size show a breakdown voltage of around −450 V as deposited, as

FIG. 3. Diode reverse leakage current at −100 V after forward bias step-stressed at various voltages for 1 min at 95% duty cycle.
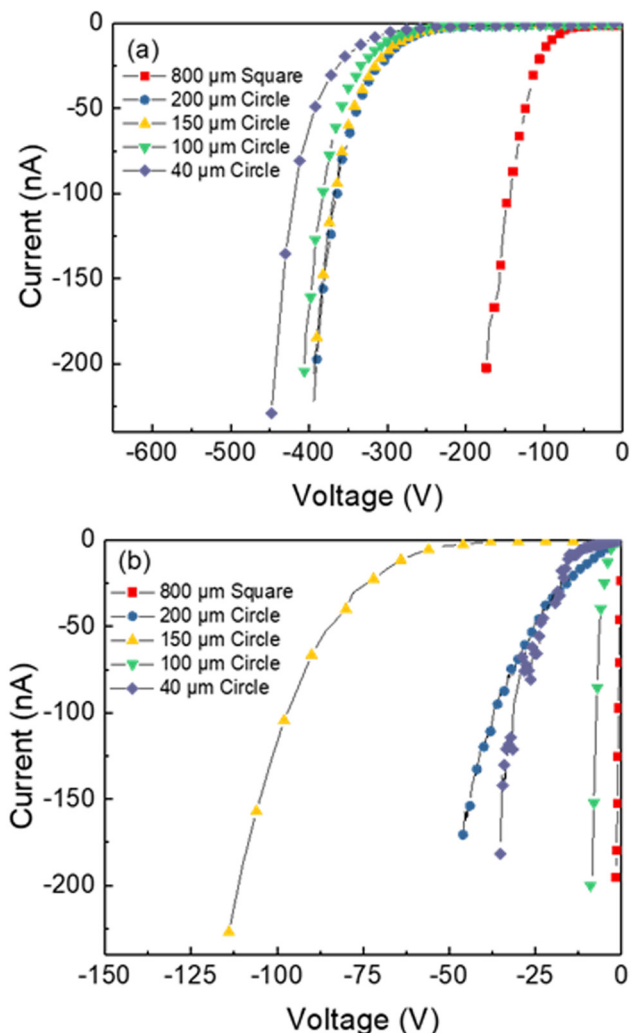
FIG. 4. Diode reverse I-V characteristics before (a) and after (b) diode failure.
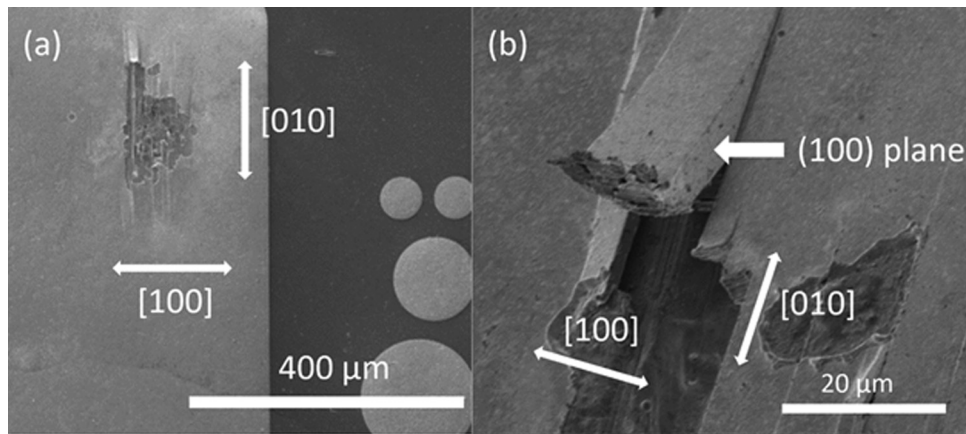
FIG. 5. SEM image for deliberately induced rupture on the Schottky contact at a high forward current condition without tilt (a) and with 45° tilting (b).

defined by a leakage current compliance of 200 nA for different sized devices, and the reverse leakage current increased irreversibly after diode forward biased at a specific forward current density, evident by the end point of Fig. 3. The breakdown current density is of 3.13×10^{-4} mA/mm^2 for 800 μm square and 1.59×10^{-1} mA/mm^2 for 40 μm circle, respectively. The reverse breakdown voltage irreversibly degrades after diode forward bias at a specific forward current density. This leads to a significant decrease in reverse breakdown voltage, e.g., in the 150 μm diameter circular devices, the breakdown decreases from ~400 to ~100 V as a result of the forward bias stressing. The electrical stressing leads to the creation of defects that degrade the device performance, manifested in a decrease in breakdown voltage. The percentage decrease is a function of device size and shape.

Figures 5(a) and 5(b) show the SEM images for 800 μm square rectifiers that failed after applying >1 A forward current at a pulsed sweep condition. There are multiple crack lines observed along the [010] direction, as shown in Fig. 5(a). The diode on-resistance mainly results from the low doped 10 μm epilayer, and the majority of diode heat generation is in this 10 μm region under forward bias conditions. Due to the low heat conductance of Ga$_2$O$_3$, heat is not properly dissipated, and the epilayer ruptures, exposing the (100) surface. Hwang *et al.* have reported the facile cleavage on the (001) and (100) planes, which corresponds to the cracks in the epilayer and the substrate observed on the [010] direction in this work.[34] Ahn *et al.* have also investigated the crack generation mechanism under ultrafast laser irradiation, showing the heat generation and stress released induces failure at natural cleavage planes.[35] Due to the low doping in the epilayer, it is expected that the Joule heating in the epilayer under high current density conditions will be the dominant contributor to device self-heating, in addition to the low thermal conductivity at elevated temperature and subsequently causing nonuniformity in thermal expansion in the epi-substrate interface and plastic deformation.[29,36–38]

Figure 6 shows that the low thermal conductivity for β-Ga$_2$O$_3$ remains the key limitation in thermal management, especially for vertical geometry devices, which is preferable for high current density applications.[37] Ahman *et al.* reported

a large anisotropy in many parameters of monoclinic β-Ga$_2$O$_3$ with a lattice constant of a = 12.21 Å, b = 3.037 Å, c = 5.798 Å with β = 103.8°.[38,39] It has been reported that the anisotropic thermal conductivity differs greatly between the low index crystallographic direction, where the [010] direction has a thermal conductivity of 21 W/m K, almost double the value of the [100] direction (10.9 W/m K).[5–7] In addition to the low room temperature thermal conductivity compared to other wide bandgap materials, the thermal conductivity along [001], [010], and [100] directions deteriorates to below 10 W/m K at elevated temperature following ~1/T relationships, as shown in Table I, and these relationships were used for thermal simulation in this work.

Figure 7 shows a thermal image for a rectifier biased at pulsed forward bias conditions. An oval pattern for temperature gradient was observed along the [100] and [010] directions in the substrate, confirming the significant anisotropic nature of thermal conductivities. Figure 8(a) shows the steady state thermal simulation temperature profile on the epi surface for a 200 μm sized rectifier biased at the corresponding failure
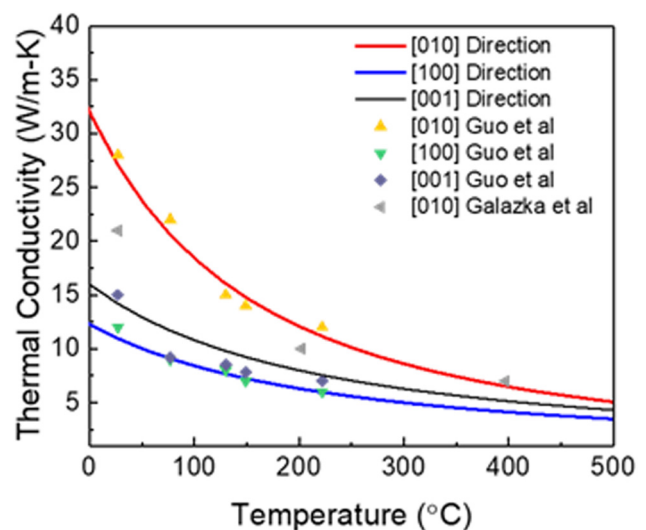

FIG. 6. Thermal conductivity values and correlations used for simulation at [100], [010], and [001] directions.
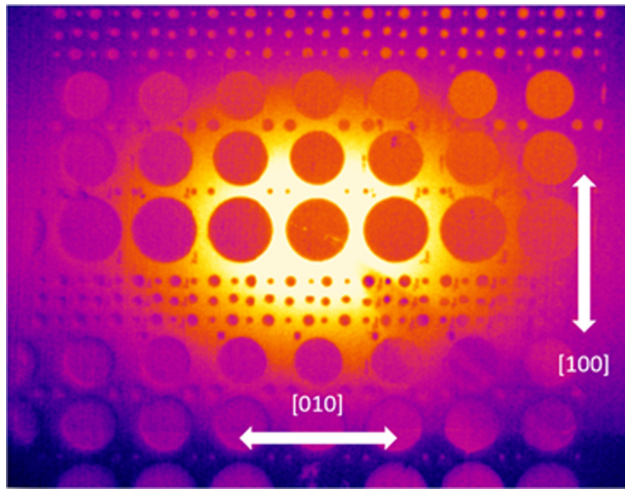
FIG. 7. Oval-shaped temperature profile captured with an infrared camera for a 1200 μm vertical diode under forward voltage bias.

condition, where similar oval patterns adjacent to the contact can also be observed, consistent with the temperature profile captured on an actual sample, as shown in Fig. 7. Figure 8(b) illustrates the vertical cross-sectional temperature contour of a rectifier, where the heat generated during steady state diode
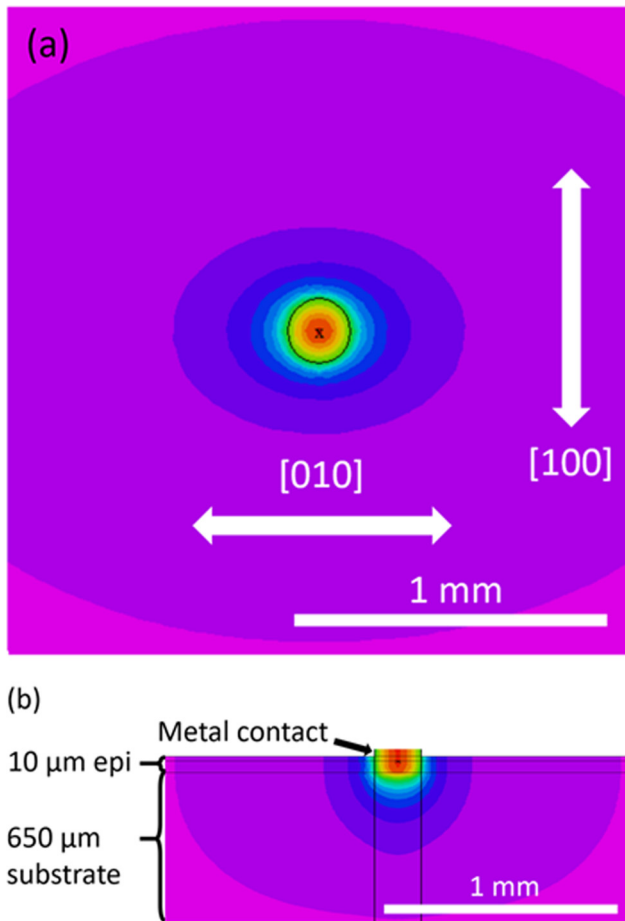

FIG. 8. Simulated temperature profile for a 200-μm size device at failure on sample surface (a) and vertical cross section (b).
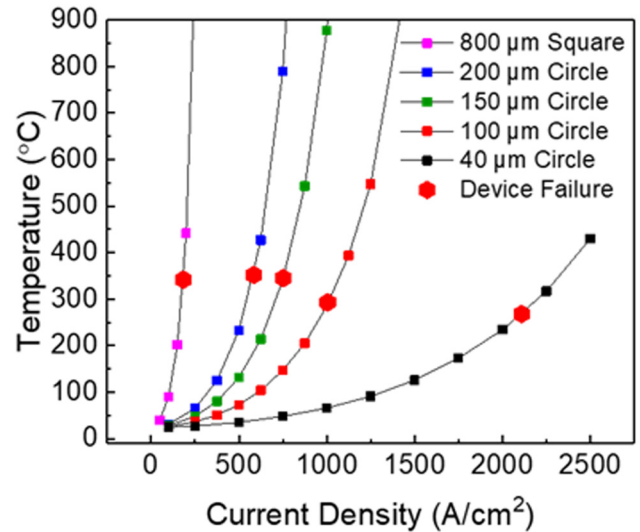

FIG. 9. Maximum junction temperature on metal surface vs current density for various device sizes.

operation is mostly concentrated on the epilayer, and potentially causing different degrees of thermal expansion at the epi-substrate interface. Chatterjee *et al.* have recently reported *in situ* Ramen mapping for device cross section for β-Ga$_2$O$_3$ Schottky rectifiers and have confirmed the concentrated heat generation near the anode/Ga$_2$O$_3$ interface.[18]

Figure 9 shows the simulated maximum junction temperatures as a function of rectifier current density for various sizes of diodes. For the same current density, higher temperature is obtained for larger sized devices, due to the larger physical volume for the epi and longer heat dissipation pathway through the device periphery. The large hexagonal symbols in each simulated curve indicate the simulated junction temperature of rectifiers biased at the condition of diode failure, as illustrated in Fig. 2(b). Although the maximum junction temperature increases in an exponential manner with respect to current density, diode failure occurs in the temperature range of 270–350 °C for all the diodes. It has been previously reported that Ni/Au Schottky contacts will fail after the Schottky metal being annealed at temperature >350 °C.[40] The low thermal conductivity causes rapid accumulation of heat at high current density operation at high temperature operation and eventually induces device failure with increased current density. Table II summarizes the

TABLE II. Current, current density, and maximum junction temperature at device failure conditions.

Device size	Current (A)	Area (cm^2)	Current density (A/cm^2)	Junction temperature at device failure (°C)
800 μm Square	1.178	6.4×10^{-3}	184	342
200 μm Circle	0.184	3.1×10^{-4}	585	352
150 μm Circle	0.133	1.8×10^{-4}	753	345
100 μm Circle	0.079	7.9×10^{-5}	1006	293
40 μm Circle	0.027	1.3×10^{-5}	2109	268

maximum temperature at device reverse degradation for various rectifier contact sizes. Constant current density has been assumed throughout this work, and due to spreading resistance on the metal contact, the current crowding effect due to probing might lead to localized high current density and overheating, which could lead to further elevation of junction temperature in the vicinity of the probe. To mitigate heating at the Schottky junction, heat sinks constructed by diamond or other materials can be employed to dissipate heat, as demonstrated in other wide bandgap materials.[31] Sharma *et al.* have performed simulations on the copper block and finned type heat sinks incorporated on the Schottky contact, and both configurations have found to be efficient in facilitating heat loss during steady state operation, compared to natural free convection simulations.[30]

V. SUMMARY AND CONCLUSIONS

We report that the degradation mechanism in the state-of-the-art β-Ga$_2$O$_3$ vertical Schottky rectifiers operating at high current >1 A and high current density >2 kA/cm^2 in reverse breakdown is plastic crystallographic deformation near the epi-substrate interface. The low doped drift region and small thermal conductivity lead to rapid heat aggregation near the epilayer and different levels of thermal expansion between the drift region and the substrate according to thermal simulations. The anisotropic nature of the thermal conductivity has been captured using an IR camera, and it should be of interest to fabricate asymmetrical devices on various epitaxial surface orientations to further optimize for stable operation for high current rectifiers. These results have also confirmed that effective thermal management is still needed in the optimization of high current density Schottky rectifiers.

ACKNOWLEDGMENTS

[1]S. J. Pearton, J. Yang, P. H. Cary, F. Ren, J. Kim, M. J. Tadjer, and M. A. Mastro, Appl. Phys. Rev. **5**, 011301 (2018).

[2]M. Higashiwaki, K. Sasaki, H. Murakami, Y. Kumagai, A. Koukitu, A. Kuramata, T. Masui, and S. Yamakoshi, Semicond. Sci. Technol. **31**, 034001 (2016).

[3]H. von Wenckstern, Adv. Electron. Mater. **3**, 1600350 (2017).

[4]S. I. Stepanov, V. I. Nikolaev, V. E. Bougrov, and A. E. Romanov, Rev. Adv. Mater. Sci. **44**, 63 (2016), available at http://www.ipme.ru/e-journals/RAMS/no_14416/06_14416_stepanov.pdf.

[5]Z. Guo *et al.*, Appl. Phys. Lett. **106**, 111909 (2015).

[6]M. Slomski, N. Blumenschein, P. P. Paskov, J. F. Muth, and T. Paskova, J. Appl. Phys. **121**, 235104 (2017).

[7]M. D. Santia, N. Tandon, and J. D. Albrecht, Appl. Phys. Lett. **107**, 041907 (2015).

[8]Z. Galazka *et al.*, J. Cryst. Growth **404**, 184 (2014).

[9]K. Konishi, K. Goto, H. Murakami, Y. Kumagai, A. Kuramata, S. Yamakoshi, and M. Higashiwaki, Appl. Phys. Lett. **110**, 103506 (2017).

[10]K. Sasaki, D. Wakimoto, Q. T. Thieu, Y. Koishikawa, A. Kuramata, M. Higashiwaki, and S. Yamakoshi, IEEE Electron Device Lett. **38**, 783 (2017).

[11]J. Yang, F. Ren, M. Tadjer, S. J. Pearton, and A. Kuramata, ECS J. Solid State Sci. Technol. **7**, Q92 (2018).

[12]Z. Hu *et al.*, IEEE Electron Device Lett. **39**, 1564 (2018).

[13]J. Yang, F. Ren, Y. T. Chen, Y. T. Liao, C. W. Chang, J. Lin, M. J. Tadjer, S. J. Pearton, and A. Kuramata, IEEE J. Electron Devices Soc. **7**, 57 (2019).

[14]Z. Hu, H. Zhou, K. Dang, Y. Z. Cai Feng, Y. Gao, Q. Feng, J. Zhang, and Y. Hao, IEEE J. Electron Devices Soc. **6**, 815 (2018).

[15]C. Joishi, S. Rafique, Z. Xia, L. Han, S. Krishnamoorthy, Y. Zhang, S. Lodha, H. Zhao, and S. Rajan, Appl. Phys. Express **11**, 031101 (2018).

[16]W. Li *et al.*, *IEDM Technical Digest, IEDM Technical Digest* (IEEE, New York, 2018), pp. 8.5.1–8.5.4.

[17]J. W. Pomeroy *et al.*, IEEE Electron Dev. Lett. **40**, 189 (2019).

[18]B. Chatterjee, A. Jayawardena, E. Heller, D. W. Snyder, S. Dhar, and S. Choi, Rev. Sci. Instrum. **89**, 114903 (2018).

[19]H. Zhou, K. Maize, G. Qiu, A. Shakouri, and P. D. Ye, Appl. Phys. Lett. **111**, 092102 (2017).

[20]Z. Cheng, L. Yates, J. Shi, M. J. Tadjer, K. D. Hobart, and S. Graham, APL Mater. **7**, 031118 (2019).

[21]C.-H. Lin, N. Hatta, K. Konishi, S. Watanabe, A. Kuramata, K. Yagi, and M. Higashiwaki, Appl. Phys. Lett. **114**, 032103 (2019).

[22]Q. He *et al.*, IEEE Electron Device Lett. **39**, 556 (2018).

[23]M. H. Wong, Y. Morikawa, K. Sasaki, A. Kuramata, S. Yamakoshi, and M. Higashiwaki, Appl. Phys. Lett. **109**, 193503 (2016).

[24]Noah Allen, Ming Xiao, Xiaodong Yan, Kohei Sasaki, Marko J. Tadjer, Jiahui Ma, Ruizhe Zhang, Han Wang, and Yuhao Zhang, IEEE Electron Device Lett. **40**, 1399 (2019).

[25]J. Noh *et al.*, IEEE J. Electron Devices Soc. **7**, 914 (2019).

[26]J. Yang *et al.*, Appl. Phys. Lett. **114**, 232106 (2019).

[27]J. Yang, F. Ren, M. Tadjer, S. J. Pearton, and A. Kuramata, AIP Adv. **8**, 055026 (2018).

[28]J. Yang, S. Ahn, F. Ren, S. J. Pearton, S. Jang, and A. Kuramata, IEEE Electron Device Lett. **38**, 906 (2017).

[29]J. Yang *et al.*, ECS J. Solid State Sci. Technol. **8**, Q3028 (2019).

[30]R. Sharma, E. Patrick, M. E. Law, J. Yang, F. Ren, and S. J. Pearton, ECS J. Solid State Sci. Technol. **8**, Q3195 (2019).

[31]T. J. Anderson *et al.*, ECS J. Solid State Sci. Technol. **6**, Q3036 (2017).

[32]J. Yang, C. Fares, F. Ren, R. Sharma, E. Patrick, M. E. Law, S. J. Pearton, and A. Kuramata, J. Appl. Phys. **123**, 165706 (2018).

[33]Y. Yao, R. Gangireddy, J. Kim, K. K. Das, R. F. Davis, and L. M. Porter, J. Vac. Sci. Technol. B **35**, 03D113 (2017).

[34]W. S. Hwang *et al.*, Appl. Phys. Lett. **104**, 203111 (2014).

[35]M. Ahn, A. Sarracino, A. Ansari, B. Torralva, S. Yalisove, and J. Phillips, J. Appl. Phys. **125**, 223104 (2019).

[36]F. Orlandi, F. Mezzadri, G. Calestani, F. Boschi, and R. Fornari, Appl. Phys. Express **8**, 111101 (2015).

[37]J. Yang, F. Ren, S. J. Pearton, and A. Kuramata, IEEE Trans. Electron Devices **65**, 2790 (2018).

[38]J. Åhman, G. Svensson, and J. Albertsson, Acta Crystallogr. Sect. C **C52**, 1336 (1996).

[39]S. K. Barman and M. N. Huda, Phys. Status Solidi **13**, 1800554 (2019).

[40]J. Yang, Z. Sparks, F. Ren, S. J. Pearton, and M. Tadjer, J. Vac. Sci. Technol. B **36**, 061201 (2018).